Catalysis Science & Technology

Accepted Manuscript

ROYAL SOCIETY OF CHEMISTRY

www.rsc.org/catalysis

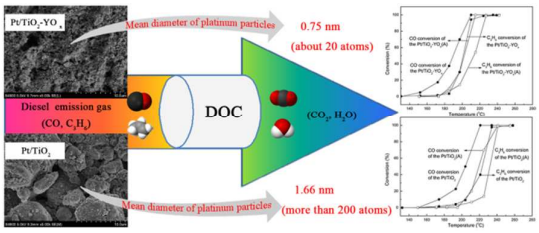

Yttria in Pt/TiO_2 catalyst improved the Pt dispersion and stabilized the structure, and hence enhanced the low-temperature activity and stability.

Effect of Yttria in Pt/TiO_2 on Sulfur Resistance Diesel Oxidation Catalyst: Enhancement of Low-Temperature Activity and Stability

Zhengzheng Yang[1], Na Zhang[2], Yi Cao[2], Maochu Gong[2], Ming Zhao[2,*], Yaoqiang Chen[1,2,*]

[1] College of Architecture and Environment, Sichuan University, Chengdu 610064, Sichuan, PR China

[2] Key Laboratory of Green Chemistry & Technology of the Ministry of Education, College of Chemistry, Sichuan University, Chengdu 610064, Sichuan, PR China

*Corresponding authors: Prof. Ming Zhao and Prof. Yaoqiang Chen

E-mail: zhaoming@scu.edu.cn (M. Zhao);

nic7501@scu.edu.cn (Y. Chen)

Tel.: +86 28 85418451; Fax: +86 28 85418451

Abstract

Compared to Pt/TiO_2, Yttria-doped Pt/TiO_2 (Pt/TiO_2-YO_x) was found to efficiently improve the activity and stability, as well as maintain the native excellent sulfur resistance of TiO_2-based catalysts unaffected. The catalysts were prepared by using co-precipitation and impregnation methods, sequentially. The as-prepared catalysts were characterized by X-ray diffraction (XRD), scanning electron microscope (SEM), N_2 adsorption-desorption, X-ray photoelectron spectroscopy (XPS), and transmission electron microscope (TEM). For Pt/TiO_2-YO_x catalysts, TEM images show that ultrafine platinum nanoparticles (<1 nm) with a narrow size distribution (0.31-1.29 nm) were dispersed on TiO_2-YO_x supports and XRD measurements confirm yttria addition could lead to suppression of the anatase crystal growth and phase transition which could consequently enhance the platinum dispersion. SEM and nitrogen adsorption-desorption results further demonstrate that the presence of yttria could stabilize the porous structure and enlarge the specific surface area of TiO_2. Hence, this work shows yttria can act as dispersion promoter and structure stabilizer, which is beneficial to low-temperature DOC activity and stability.

Keywords: Pt/TiO_2-YO_x, DOC, sulfur resistance, ultrafine platinum nanoparticles, high specific surface area

1. Introduction

Diesel engine emissions, such as gas phase nitrogen oxides (NO_x), particulate matter (PM), unburned hydrocarbons (HC) and carbon monoxide (CO), are considered a major source of air pollutants. Due to the large oxygen excess, sulfur dioxide, and vapor in the exhaust, conventional three-way catalysts (TWCs) alone cannot clean these pollutants effectively.[1] In order to meet increasingly stringent regulations imposed by government agencies, a common integrated emission control system containing diesel oxidation catalyst (DOC) + catalyzed diesel particulate filter (CDPF) + selective catalytic reduction (SCR) has seen increased utilization recently.[2-5] In such integrated emission control systems, DOC has been functionalized as a remover for CO, HC and the soluble organic fraction (SOF) of particulates.

In recent years, commercial DOC technology has been developed and has been mainly based on Pt/Al_2O_3[6,7] and $Pt\text{-}Pd/CeO_2\text{-}ZrO_2\text{-}Al_2O_3$.[3,8,9] Although these kinds of catalysts exhibit a high activity, their sulfur poisoning resistance performance was poor.[10-16] Due to the fact that sulfur is present in all commercial fuels, especially in developing countries, sulfur content in commercial diesel fuels is extremely high,[17-19] it is an urgent matter to solve the DOC sulfur poisoning phenomenon in these areas.[2,20,21]

To deal with the problem of high sulfur level in commercial diesel

fuels, a non-sulfating support,[22] TiO_2, has been employed as an effective sulfur resistance component for the development of new vehicle exhaust catalysts.[1,23-27] However, TiO_2 has a smaller specific surface area which results in low CO and HC performance as well as poor thermal stability for Pt sintering and deterioration of catalytic activity.[28] This is especially true in the described integrated diesel emission control system where during active DPF regeneration; the DOC temperature can reach upwards of 850 ^{o}C.[2,29] Thus, it is important to improve the specific surface area and thermal stability which is favorable for DOC activity.

In this study, a Pt/TiO_2-YO_x catalyst was prepared and the promotion effects of yttria on the catalytic performance and thermal stability of Pt/TiO_2 sulfur resistance DOC were studied.

2. Experimental

2.1. Catalyst preparation

The TiO_2-YO_x mixed oxides were prepared by co-precipitation with the molar ratio of Ti : Y = 9 : 1, which was the optimal ratio in our previous study.[30] Desired $TiOSO_4 \cdot 2H_2O$ and $Y(NO_3)_3 \cdot 6H_2O$ mixture solutions were slowly added to $NH_3 \cdot H_2O$ solutions under vigorous stirring. The precipitate was then filtered and washed many times. After drying and calcining for 3h at 500 ^{o}C under airflow, the TiO_2-YO_x mixed

oxides powder was obtained. The TiO_2 support was also prepared by the same method.

The Pt/TiO_2-YO_x catalyst was prepared using incipient impregnation method. $(EA)_2Pt(OH)_6$ solution was impregnated on TiO_2-YO_x mixed oxides support with the mass ratio of Pt: TiO_2-YO_x = 1.0 wt%. After drying for 2h at 120 ^oC and baking for 2h at 400 ^oC under airflow, the catalyst powders were ball milled with binding material (1.0 wt.%, $ZrO(Ac)_2$) to form a slurry. Then, the resulting slurry was coated onto ceramic honeycomb (400 cell/inch^2, Corning, America). The loading of washcoat was kept about 120 g/L. After drying overnight at 120 ^oC and calcining for 2h at 400 ^oC under airflow, the monolithic catalyst was obtained. The Pt/TiO_2 catalyst was prepared by the same method.

Pt/Al_2O_3 and Pt-Pd/CeO_2-ZrO_2-Al_2O_3 commercial DOC catalysts were supplied by Sichuan Zhongzi Exhaust Purge Co. Ltd.

To investigate sulfur resistance, the fresh catalysts were sulfur poisoned in 1250 ppm SO_2, 5% O_2, 0.62% vapor and N_2 balance gas at 450 ^oC for 60 min,[28] the only difference is that we extended the treatment time to 2.5 h so as to simulate the effect of long-term use of high sulfur level diesel fuels on the catalyst. The sulfur poisoned samples were marked as Pt/TiO_2(S), Pt/TiO_2-YO_x(S), Pt/Al_2O_3(S) and Pt-Pd/CeO_2-ZrO_2-Al_2O_3(S).

To simulate the influences of vehicle long-term use, the fresh catalysts

were placed in the reactor and aged at 670 ^{o}C for 15h and then at 250 ^{o}C for 15h in the aging gases containing C_3H_6: 600 ppm, CO: 1500 ppm, NO: 200 ppm, SO_2: 50 ppm, O_2: 5%, CO_2: 4%, vapor: 8%, N_2: balance, flow rate: 800 mL/min. This aging process fits well with vehicle aging at 160,000 km,[31] and it sufficient for aging TiO_2 based catalysts.[32] The aged samples were named as Pt/TiO_2(A), Pt/TiO_2-YO_x(A), Pt/Al_2O_3(A) and Pt-Pd/CeO_2-ZrO_2-Al_2O_3(A).

2.2. Catalyst characterization

The nitrogen adsorption-desorption isotherms were performed on QUADRASORB SI automated surface area and pore size analyzer (Quantachrome Instruments) at liquid nitrogen temperature. The specific surface area and pore size measurements were calculated by Brunauer-Emmett-Teller (BET) method and Barret-Joyner-Halenda (BJH) method, respectively. Before adsorption measurements, the samples were degassed at 300 ^{o}C for 3h under vacuum.

The morphologies of catalysts were observed using scanning electron microscopy (SEM) S-4800 (Hitachi Ltd.) operated at 5 kV. To observe the surface of washcoat, the monolithic catalysts were cut, and then detected. The sulfur content deposition of each catalyst was analyzed using an energy-dispersive X-ray (EDX) spectroscopy IE-250 (Oxford Instruments).

X-ray diffraction (XRD) patterns of the samples were collected by powder X-ray diffraction on a DX-1000 diffractometer using Cu Kα radiation (λ = 0.15418 nm) operated at 40 kV and 25 mA. The XRD data were recorded for 2θ values from 10^o to 80^o with an interval of 0.03^o. The crystalline phases were identified by comparison with the reference from International Center for Diffraction Data (ICDD).

X-ray photoelectron spectra (XPS) data were collected on a Kratos XSAM 800 spectrometer (Kratos Analytic Inc.) with Al Kα radiation operated at 15 kV and 12 mA, calibrating internally by the C1s binding energy (BE) 284.8 eV.

2.3. Catalytic activity measurements

The catalytic activity measurements were performed in a multiple fixed bed continuous flow reactor. The monolithic catalysts were placed in a tubular quartz reactor with a surrounding electrical heating coil. The simulated diesel engine exhaust[33] was controlled by mass flow controllers before entering blender, and contained a mixture of NO: 200 ppm, C_3H_6: 330 ppm, CO: 1000 ppm, O_2: 10%, CO_2: 8%, vapor: 7%, 50 ppm SO_2 (it amounts to diesel fuels with about 1000 ppm of sulfur[7,34]) and N_2 balance, the gas space velocity was 60,000 h^{-1}. The catalyst bed temperature was measured in the middle of one of the center channels inside the monolith catalyst[31] by a 0.5 mm K-thermocouple. The inlet gas temperature was

measured by another thermocouple, in order to avoid the effect of catalytic oxidation reactions (exothermic reactions) to inlet gas temperature, the thermocouple was fixed 20 mm in front of the monolith.

The outlet C_3H_6 was analyzed with a GC2000II online gas chromatograph (Shanghai Analysis Instruments, China) using a flame ionization detector (FID), CO was analyzed with an FGA-4100 automotive emission analyzer (Foshan Analytical Instrument Co., Ltd, China), NO and NO_2 was detected by FT-IR (Antaris IGS, Nicolet, USA).

3. Results and discussion

3.1. Catalytic performance and sulfur resistibility

3.1.1. Catalytic activity and stability

Fig. 1 shows CO and C_3H_6 conversion over fresh and aged catalysts. Fresh Pt/TiO_2-YO_x catalyst shows CO 50% conversion (T_{50}) at around 190 ^oC, while for Pt/TiO_2, the light-off temperature (T_{50}) rises to around 204 ^oC. For C_3H_6 conversion activity, Pt/TiO_2-YO_x is also better than Pt/TiO_2, the light-off temperature over Pt/TiO_2-YO_x is 201 ^oC, while for Pt/TiO_2 catalyst, the value increases to 223 ^oC. After implementing the 160,000 km vehicle aging treatment protocol,[31] the aged catalyst

Pt/TiO_2-YO_x(A) shows 50% CO and C_3H_6 conversion at around 202 ^oC and 213 ^oC, respectively. The light-off temperature of CO and C_3H_6 over Pt/TiO_2(A) catalyst are 219 ^oC and 232 ^oC, respectively. It can be seen that, the CO and C_3H_6 T_{50} of fresh Pt/TiO_2-YO_x are 14 ^oC and 22 ^oC lower than that of fresh Pt/TiO_2, and the CO and C_3H_6 T_{50} of Pt/TiO_2-YO_x(A) are 17 ^oC and 19 ^oC lower than Pt/TiO_2(A). In all cases, the presence of yttria is beneficial to the catalytic efficiency of CO and C_3H_6.

According to the above results, the oxidation activities of C_3H_6 and CO are both decreasing after the vehicle aging treatment, which may result from sulfur accumulation or platinum particle sintering after long-term use.[31,35,36] Also, C_3H_6 oxidation activity is inferior compared to CO, which may be explained by the fact that C_3H_6 oxidation occurs after the CO has been removed from the active component surfaces.[37-39]

3.1.2. Sulfur resistibility

Catalytic activities over the catalysts before and after sulfur-poisoning treatment are shown in Fig. 2. The sulfur-poisoning influence on the catalytic activity of Pt/TiO_2 and Pt/TiO_2-YO_x are both slight. The light-off temperature (T_{50}) of CO over fresh Pt/TiO_2-YO_x catalyst is about 190 ^oC, and for the sulfur-poisoning treatment sample Pt/TiO_2-YO_x(S) the value is 192 ^oC, the difference is just 2 ^oC. For the

Pt/TiO_2 catalyst, sulfur-poisoning treatment only lead to about 3 ^oC T_{50} (CO) difference. The C_3H_6 T_{50} increment over both Pt/TiO_2-YO_x and Pt/TiO_2 are negligible after the sulfur-poisoning treated. For a comparison of as-prepared catalysts, commercial DOC catalysts such as Pt/Al_2O_3 and $Pt\text{-}Pd/CeO_2\text{-}ZrO_2\text{-}Al_2O_3$ were also tested by the same sulfur-poisoning routine, which leads to 23 ^oC and 7 ^oC CO T_{50} differences, respectively. As well, the light-off temperature of C_3H_6 over Pt/Al_2O_3 and $Pt\text{-}Pd/CeO_2\text{-}ZrO_2\text{-}Al_2O_3$ are both increased by 8 ^oC due to the sulfur-poisoned (Supporting Information Fig.1). This implies that the same sulfur-poisoning treatment process leads to more severe deactivation of commercial DOC than as-prepared catalysts. In addition, the sulfur content deposited on each catalyst was analyzed using EDX and results are shown in Table 1. Sulfur content deposited on Pt/TiO_2(A) and Pt/TiO_2(S) are 1.3 wt.% and 1.7 wt.%, respectively. For Pt/TiO_2-YO_x(A) and Pt/TiO_2-YO_x(S), the values are 1.8 wt.% and 2.3 wt.%, respectively. However, for Pt/Al_2O_3(A), Pt/Al_2O_3(S) and $Pt\text{-}Pd/CeO_2\text{-}ZrO_2\text{-}Al_2O_3$(A), $Pt\text{-}Pd/CeO_2\text{-}ZrO_2\text{-}Al_2O_3$(S) commercial catalysts, the values are 5.8 wt.%, 5.8 wt.% and 4.4 wt.%, 4.8 wt.% respectively. Results indicate that TiO_2-based (both Pt/TiO_2 and Pt/TiO_2-YO_x) DOC catalysts show better sulfur resistance performance than recent Pt/Al_2O_3 and $Pt\text{-}Pd/CeO_2\text{-}ZrO_2\text{-}Al_2O_3$ commercial DOCs. However, the effect of Y addition on sulfur resistibility is not significantly

distinct according to the EDX analysis.

3.1.3. Kinetics

In order to clearly clarify the activity differences between the catalysts the apparent activation energy (Ea) has been calculated from Arrhenius plots of ln(TOF) vs 1000/T (T: Catalyst bed temperature) for C_3H_6 and CO oxidizing reaction (Fig. 3) and listed in Table 2. A higher space velocity (60,000 h^{-1}) as well as low CO and C_3H_6 conversions (less than 25%) was selected to achieve the kinetically controlled conditions. The rate of the reactions was calculated by using the equation:

$$\text{rate} = \frac{FX}{\upsilon W},$$

where F is the inlet molar flow rate of the particular gas, X is the fractional conversion of gas at a particular temperature, υ is the stoichiometric coefficient of the gas, and W is the weight of the catalyst.[40]

As listed in Table 2, the reaction rate of CO oxidation at 190 ^oC (catalyst bed temperature) over Pt/TiO_2-YO_x is 1.97×10^{-6} mol g^{-1} s^{-1}, which is significantly higher than that on Pt/TiO_2 (1.40×10^{-6} mol g^{-1} s^{-1}). For the C_3H_6 oxidation reaction, this phenomenon is more evident, the reaction rate at 205 ^oC (catalyst bed temperature) over Pt/TiO_2-YO_x is 5.73×10^{-7} mol g^{-1} s^{-1}, which is almost four greater than on the Pt/TiO_2 catalyst (1.51×10^{-7} mol g^{-1} s^{-1}). The turnover frequency (TOF, which is the number of CO or C_3H_6 molecule converted per Pt per second) with

respect to the total platinum content on catalyst shows a similar trend. Fig. 3 shows the Arrhenius plots of the TOF for CO + O_2 and C_3H_6 + O_2 reactions with respect to the total Pt amount. There is a remarkable difference in apparent activation energy between Pt/TiO_2-YO_x and Pt/TiO_2 catalysts. The CO + O_2 reaction over Pt/TiO_2-YO_x is about 78.6 kJ mol^{-1}; however, for Pt/TiO_2 catalyst it is about 182.1 kJ mol^{-1}. Results indicate that the addition of yttria improved the CO catalytic activity of Pt/TiO_2 DOC catalyst. For the C_3H_6 + O_2 reaction over Pt/TiO_2-YO_x and Pt/TiO_2 the apparent activation energies are about 155.2 and 197.0 kJ mol^{-1}, respectively. We found our calculated activation energy of C_3H_6 over Pt/TiO_2-YO_x is apparently smaller than that over Pt/TiO_2, which indicates the yttria improved catalytic activity of C_3H_6 over Pt/TiO_2-YO_x. Compared with the Ea (C_3H_6) over Pt/Al_2O_3 (143.9 kJ/mol) (few studies focusing on Ea (C_3H_6) over Pt/TiO_2) reported by Oh et.,[41] we found our calculated Ea(C_3H_6) is a little bit larger than the literature. Whether such comparison is directly related is under a debate and need for further investigation.

After rigorous sulfur-poisoning treatment, Ea (CO) and Ea (C_3H_6) over Pt/TiO_2(S) are 182.7 and 198.1 kJ mol^{-1}, respectively, which shows just 0.6 and 1.1 kJ mol^{-1} increment than fresh Pt/TiO_2 catalyst. For Pt/TiO_2-YO_x(S), Ea (CO) and Ea (C_3H_6) are 95.6 and 165.5 kJ mol^{-1}, compared with fresh Pt/TiO_2-YO_x catalyst, the increment is just 17.0 and

10.3 kJ mol^{-1}, respectively. It can be seen that, the catalyst deactivation of Pt/TiO_2 and Pt/TiO_2-YO_x caused by sulfur poisoning is slight. For Pt/Al_2O_3 and Pt-Pd/CeO_2-ZrO_2-Al_2O_3 commercial DOC catalyst (Supporting Information Fig.2 and Table 1), the sulfur treatment nearly reduced the reaction rate and TOF for both CO + O_2 and C_3H_6 + O_2 reactions by half. Likewise, the CO + O_2 reaction apparent activation energy over Pt/Al_2O_3 is about 53.9 kJ mol^{-1}, which is consistent with reference,[40] and the value has almost doubled due to the sulfur treatment. The apparent activation energy of the CO + O_2 reaction over Pt-Pd/CeO_2-ZrO_2-Al_2O_3 is about 82.8 kJ mol^{-1}, which increased to 145.7 kJ mol^{-1} after sulfur treatment. Moreover, the C_3H_6 + O_2 reactions apparent activation energy over both Pt/Al_2O_3(S) and Pt-Pd/CeO_2-ZrO_2-Al_2O_3(S) also shows the similar trend. It can be seen that sulfur-poisoning treatment leads to the decrease of catalytic performance and increase of apparent activation energy, which caused by that sulfur-poisoning treatment would lead to activation barrier increases, when sulfur is absorbed on the surface of the catalyst.[42] Due to sulfur is absorbed on the surface of the catalyst which would lead to exposed Pt decreases, using total Pt to calculate the Ea of sulfur-poisoned samples may lead to pre-exponential factor changing and Ea value higher, Olsson et. al.[43-49] using exposed Pt to calculate the kinetic parameters is more precise. In addition, this phenomenon about sulfur-poisoning would be

relieved if appropriate pre-treatment (such as 800 °C H_2 reduction), Dawody and Olsson et. al. indicate[50-53] that the sulfur species on sulfur-poisoned catalysts would be desorbed after H_2 high temperature treatment. Based on the previous analysis it can be proved that, TiO_2-based DOC catalysts (both Pt/TiO_2 and Pt/TiO_2-YO_x) show better sulfur resistance than recent Pt/Al_2O_3 and $Pt\text{-}Pd/CeO_2\text{-}ZrO_2\text{-}Al_2O_3$ commercial DOCs.

3.1.4. NO oxidation activity

Besides CO and C_3H_6 activities, it is also important[54] to investigate NO catalytic oxidation performance by employing as-prepared DOC because higher NO_2 concentrations are beneficial for downstream soot oxidation at low temperatures,[55,56] fast SCR reaction,[57-62] and NO_x storage on the LNT.[63,64] The conversion of NO to NO_2 over Pt/TiO_2 and Pt/TiO_2-YO_x are shown in Fig. 4, the conversion is more than 30% in the temperature range of 253-334 ^oC and reachs a maximum of 45% at 278 ^oC over the Pt/TiO_2 catalyst. For Pt/TiO_2-YO_x catalyst, the temperature range, which reachs more than 30% NO conversion, is 238-334 ^oC and the conversion reaches more than 51% at 279 ^oC. Results demonstrate that the yttria-doped Pt/TiO_2 catalyst widens the low temperature range and enhances the highest conversion of NO oxidation.

To summarize, TiO_2-based DOC catalysts (both Pt/TiO_2 and

Pt/TiO_2-YO_x) show better sulfur resistance than recent commercial DOC catalysts (Pt/Al_2O_3 and $Pt\text{-}Pd/CeO_2$-ZrO_2-Al_2O_3). The addition of yttria is also beneficial for the CO, C_3H_6 and NO oxidation activity as well as stability of the Pt/TiO_2 catalyst. In order to determine how yttria affects the catalytic activity and stability of the Pt/TiO_2 catalyst, several characterization techniques were carried out.

3.2. Catalyst characterization

3.2.1. N_2 adsorption-desorption isotherms

To determine the texture properties of the catalyst supports, N_2 adsorption-desorption techniques was employed. As shown in Table 3, the pore volume and average pore size of TiO_2 and TiO_2-YO_x are similar, whereas the BET specific surface area of TiO_2 is 98 m^2/g, for TiO_2-YO_x, the BET specific surface area is 155 m^2/g. As a result, catalytic activity of Pt/TiO_2-YO_x for the DOC reaction is improved due to the larger surface area which is capable of enhancing the dispersion of the active component.[65] For both of the aged cases, the specific area decreases and average pore size increases. Interestingly, the pore volume of TiO_2 decreases drastically after high temperature calcination but the pore volume of TiO_2-YO_x(A) remains quite similar when compared with the fresh TiO_2-YO_x simple. Taking the pore size distribution (Fig. 5) into

consideration, it can be seen that, the pore size of the TiO_2 is increased, and both the specific surface areas and pore volume of TiO_2 support are decreased, which indicates that the TiO_2 support is sintered and the open pore structure is collapsed to form plugged pores during the high temperature aging process. For the TiO_2-YO_x support, after high temperature treatment the pore size is increased but the large pore volume is unchanged, which implies that the small pores is sintered to form large pores but the open pores are not collapsed to form closed pores. Thus it can be inferred that one of the reasons why the activity of Pt/TiO_2-YO_x was better than Pt/TiO_2 was that the active surface component was covered during the process of TiO_2 open pores collapse. These results are confirmed by SEM detection (Fig. 6).

3.2.2. SEM

To observe the surface morphologies of the catalysts clearly, SEM measurements were conducted. As shown in Fig. 6, lumpish particles are formed in the Pt/TiO_2 catalyst, however for the Pt/TiO_2-YO_x catalyst, the surface appearance resembles a porous spongy-like structure. Further, after synthetic aging the massive particles of Pt/TiO_2(A) catalyst increase significantly, but the porous surface structure of Pt/TiO_2-YO_x(A) catalyst is maintained. This result implies that the modification of yttria stabilized the porous structure of the TiO_2-YO_x support and suppressed the support

material particles from high temperature sintering. Moreover, due to the fact that the porous structure collapsed and support particles sintered may lead to the active component Pt sintering and imbedding which leads to the active sizes decrease as well as catalyst deactivation. Thus, Pt/TiO_2-YO_x and Pt/TiO_2-YO_x(A) catalysts with stable porous structures show better catalytic performance. In addition, because the gas and thermal diffusion process are more efficient in porous materials[66,67] and better diffusion causes better catalytic performance at high conversions, which could be another reason why Pt/TiO_2-YO_x with porous spongy-like structure catalyst shows better activity for the DOC reaction than Pt/TiO_2 catalyst with large granular structures. It can be concluded that the addition of yttria is favorable to improve and stabilize porous texture performance of the Pt/TiO_2 catalyst, which leads to enhanced activity and stability.

3.2.3. XRD

In order to investigate the phase and composition of the catalyst supports, these catalyst supports were characterized using XRD. Fig. 7 shows the XRD diffraction patterns of both fresh and aged samples. Typical anatase structure peaks are observed in all samples except in TiO_2-YO_x support, TiO_2-YO_x is mainly amorphous TiO_2 with a few anatase, and the degree of crystallinity is approximately 22.4%, but for

TiO_2 the degree of crystallinity is 76.8%. This demonstrates that the phase transition from amorphous to anatase of TiO_2 is suppressed by the addition of yttria. For aged samples, TiO_2-YO_x(A) is mainly anatase without rutile phase and the anatase average crystallite size of this sample is about 11 nm. However, for TiO_2(A), the rutile (110), (101) and (111) peaks located at 27.4, 36.1 and 41.2^o become very intense, the total amount of rutile is about 14.7 wt.%, and the average crystallite size of anatase increased to about 21 nm. This implies that the existence of yttria in TiO_2 is beneficial to suppress TiO_2 phase transitions and anatase crystal growth. The transition from anatase to rutile and anatase crystal growth often lead to the original TiO_2 texture properties being destroyed, specific surface areas decreasing and even particles sintering which is observed by both the N_2 adsorption-desorption technique as well as SEM. Furthermore specific surface area decreases and support particles sintering often lead to Pt sintering[28] and imbedding which results in deactivation. Thus, modification of yttria suppressed TiO_2 phase transition and anatase crystal growth and hence stabilized TiO_2 porous structure, improved the thermal stability of the Pt/TiO_2 catalyst, which is consistent with Ref.[68-70]

In addition, the characteristic diffraction peaks of YO_x in TiO_2-YO_x was not found, and the positions of typical anatase structure peaks shifted slightly to smaller angles, which may imply that at least part of Y ions

(Y^{3+} radius: 0.09 nm) entered the TiO_2 lattice (Ti^{4+} radius: 0.06 nm) leading to an expansion of TiO_2 unit cell. The lattice volume of the anatase tetragonal cell of TiO_2-YO_x(A) is 0.1362 nm^3, while for TiO_2 and TiO_2(A), the values are 0.1356 nm^3 and 0.1357 nm^3, respectively. It can be found that yttria entered the TiO_2 lattice and expanded the unit cell of TiO_2, and it is a possible reason why the addition of yttria suppresses the phase transformation of TiO_2.

3.2.4. XPS

The chemical state of Pt and the surface composition of the catalysts were determined using the XPS technique. As shown in Fig. 8(a), the Pt/TiO_2 catalyst shows four peaks around 72.2, 75.6, 74.8 and 78.2 eV, respectively. The peaks around 78.2 and 74.8 eV are assigned to $4f_{5/2}$ and $4f_{7/2}$ peaks of PtO_2, the $4f_{7/2}$ peak (72.2 eV) and $4f_{5/2}$ peak (75.6 eV) confirm that PtO species exist in the Pt/TiO_2 catalyst. For the Pt/TiO_2-YO_x catalyst, the $4f_{7/2}$ peak position of PtO_2 is around 74.8 eV with a spin-orbit splitting at 78.2eV, corresponding to the $4f_{5/2}$ peak of PtO_2, but the PtO state was not distinctly detected. Furthermore, metallic platinum was not detected on either the Pt/TiO_2 or Pt/TiO_2-YO_x catalyst. It can be observed that, calcination in air at high temperature leads to platinum particles existing in oxide form in both Pt/TiO_2 and Pt/TiO_2-YO_x catalysts. Taking Pt species on Pt/TiO_2 catalyst (PtO_2 and

PtO) and Pt/TiO_2-YO_x catalyst (PtO_2) into consideration, this result indicates that the addition of yttria into TiO_2 contributes to Pt particles being entirely oxidized over the catalyst easier. One possible reason for such a phenomenon is that platinum particles on the Pt/TiO_2-YO_x catalyst are smaller than on the Pt/TiO_2 catalyst due to the fact that smaller platinum particles are more easily oxidized under oxidizing atmospheres.[71-77] Similarly, the Pt/TiO_2-YO_x catalyst with smaller PtO_x particles should be reduced more easily in the presence of reducing gas, which is confirmed by the H_2-TPR profiles (Supporting Information Fig.3). Moreover, the Pt/TiO_2 and Pt/TiO_2-YO_x catalysts after 3h reaction under the simulated diesel exhaust gases were detected using XPS and shown in Fig.8(b). Results imply that Pt^0 forms on both Pt/TiO_2 and Pt/TiO_2-YO_x catalysts, the chemical states of Pt on Pt/TiO_2 are Pt^0, Pt^{2+} and Pt^{4+}, however the Pt chemical states on Pt/TiO_2-YO_x are just Pt^0 and Pt^{4+}, furthermore, the content of Pt^0 on the Pt/TiO_2-YO_x catalyst is significantly more than that on the Pt/TiO_2 catalyst. It indicates that PtO_x can be reduced under the simulated diesel exhaust gases (containing CO, C_3H_6) even it is under oxygen-rich condition, thus the presence of Y in Pt/TiO_2 catalyst is beneficial to reduce Pt^{2+} to Pt^0, and hence promoting the Pt^0 production. Generally, Y entrying into the titania lattice would create oxygen vacancies, which influence the chemical state of Pt and enhance the interaction of Pt with the support,[78] and can act as nucleation

centers which are in favor of the dispersion of the catalyst active phase.[78,79] In addition, smaller PtO_x particles also may benefit to the PtO_x reducing to form Pt^0 active component.[72] Thus the Pt/TiO_2-YO_x catalyst which forms Pt^0 active component more easily shows better catalytic activity. In order to confirm the assumption, these catalysts were characterized using TEM (Fig. 9).

In addition, titania peaks of the Pt/TiO_2 and Pt/TiO_2-YO_x catalysts are both located at 458.5 ($2p_{3/2}$) and 464.1 eV ($2p_{1/2}$), which are characteristic of TiO_2 species. Yttria peaks of the Pt/TiO_2-YO_x catalyst are located at 157.5 ($3d_{5/2}$) and 159.4 eV ($3d_{3/2}$) as shown in Fig. 8(c), which are obviously higher than the peaks of the Y_2O_3 support material ($3d_{5/2}$: 156.8 eV, $3d_{3/2}$: 158.7 eV), which were prepared and treated under the same conditions (Table 4). The characteristic peaks of Y_2O_3 species are located at 156.4 eV ($3d_{5/2}$) and 158.2 eV ($3d_{3/2}$),[80] which is close to the values of Y_2O_3 and the difference may be caused by the calibrated binding energy scales. Thus, we conjecture that yttria may exhibit strong interactions with titania and cause electron binding energy deviation. This is a possible reason why yttria modified TiO_2 shows better thermo-stability.

3.2.5. HAADF-STEM and HR-TEM

Figure 9a and b show the HAADF-STEM images of Pt/TiO_2 and

Pt/TiO_2-YO_x catalysts. It can be observed that platinum particles are highly and homogeneously dispersed on the surface of the supports. To count the platinum particle size on both catalysts clearly, high resolution TEM (Fig. 9c and d) was applied. Figure 9e shows the platinum particle size distributions for Pt/TiO_2 and Pt/TiO_2-YO_x catalysts. The particle size of platinum for the Pt/TiO_2 catalyst ranges between 0.66 and 3.03 nm, with a mean diameter of 1.66 nm, which consists of about 210 platinum atoms (sphere model calculation). For the Pt/TiO_2-YO_x catalyst, the platinum particle mean diameter is 0.75 nm, and is composed of about 20 platinum atoms which is approximately 10 times less than the Pt/TiO_2 catalyst, and the particle size distribution is in the range of 0.31-1.29 nm. It can be seen that platinum particles are dispersed on the surface of the yttria doped-TiO_2 support with smaller size. Due to the total Pt loading amount is the same, there would be more catalytic active sites and hence promoting the catalytic performance. Therefore, Pt/TiO_2-YO_x catalysts with smaller Pt particles show better catalytic activity than the Pt/TiO_2 catalyst. This result is consistent with the measurements of XPS and activity test.

4. Conclusions

Yttria addition increased the reaction rates and reduced the apparent activation energy of the Pt/TiO_2 catalyst for CO and C_3H_6 oxidation

reactions, and this trend remained significant after mimicking 160,000 km vehicle aging treatment. The light-off temperature of as-prepared Pt/TiO_2-YO_x catalyst for CO oxidation is just 190 ^oC ($T_{50,\,CO}$), for C_3H_6 oxidation T_{50,C_3H_6} and T_{70,C_3H_6} are just 201 ^oC and 205 ^oC, respectively, at a gas hourly space velocity (GHSV) of 60,000 h^{-1}. Some current patented DOC products show $T_{50,\,CO}$ at about 191-199 ^oC, T_{50,C_3H_6} at about 196-205 ^oC,[8,9] T_{70,C_3H_6} at about 202-220 ^oC[81] under similar simulated diesel engine exhaust gases constituents and 50,000 h^{-1} GHSV. And for Pt-only commercial DOC catalyst, the T_{50,C_3H_6} is 181 ^oC at 30,000 h^{-1} GHSV.[82] At 70,000 h^{-1} GHSV, the $T_{50,\,CO}$ are about 190-215 ^oC and T_{50,C_3H_6} are about 205-230 ^oC.[83] It can be seen that, the catalytic performances of as-prepared Pt/TiO_2-YO_x are similar and even better than the current commercial DOCs or patented DOC products. The effect of Y in TiO_2 on sulfur tolerance is indirect, and the Pt/TiO_2-YO_x catalyst also shows excellent sulfur resistibility. Therefore, Pt/TiO_2-YO_x catalyst shows extensive commercial potentiality and important practical significance, especially in developing countries where sulfur content in commercial diesel fuels is extremely high.

Acknowledgements

This work was supported by the National Natural Science Foundation of China (21173153) and the Major Research Program of Sichuan

Province Science and Technology Department (2011GZ0035, 2012FZ0008). The Analytical and Testing Center of Sichuan University provided TEM analysis. The authors gratefully acknowledge Junbo Zhong (Sichuan University of Science and Engineering), Jun Li (Sichuan University) and Jeffrey G Bell (University of Windsor, Canada) for language help and writing assistance. Discussions with Jun Li and Jianli Wang (Sichuan University) are greatly appreciated.

References

1 H.Y. Huang, R.Q. Long, R.T. Yang, *Appl. Catal. B: Environ.*, 2001, **33,** 127-136.

2 J. Luo, D. Kisinger, A. Abedi, W.S. Epling, *Appl. Catal. A: Gen.*, 2010, **383,** 182-191.

3 O.H. Bailey, M. Hedgecock, US patent, 0099975, 2011.

4 T. Johnson, SAE paper 2012-01-0368, 2012.

5 T. Johnson, SAE paper 2013-01-0538, 2013.

6 S. Verdier, E. Rohart, O. Larcher, V. Harle, M. Allain, SAE paper 2005-01-0476, 2005.

7 A. Russell, W.S. Epling, *Catal. Rev.-Sci. Eng.*, 2011, **53,** 337-423.

8 G. Grubert, T. Neubauer, A.H. Punke, T.W. Mueller-Stach, A. Siani, S.A. Roth, J.B. Hoke, S. Sung, Y. Li, X. Wei, M. Deeba, US patent, 2010/0180581, 2010.

9 G. Grubert, T. Neubauer, A.H. Punke, T.W. Mueller-Stach, A. Siani, S.A. Roth, J.B. Hoke, S. Sung, Y. Li, X. Wei, M. Deeba, US patent, 8211392, 2012.

10 S.S. Deshmukh, M. Zhang, V.I. Kovalchuk, J.L. d'Itri, *Appl. Catal. B: Environ.*, 2003, **45,** 135-145.

11 T. Luo, R.J. Gorte, *Appl. Catal. B: Environ.*, 2004, **53,** 77-85.

12 F.C. Galisteo, R. Mariscal, M.L. Granados, M.D.Z. Poves, J.L.G. Fierro, V. Kröger, R.L. Keiski, *Appl. Catal. B: Environ.*, 2007, **72,** 272-281.

13 T. Kolli, M. Huuhtanen, A. Hallikainen, K. Kallinen, R. L. Keiski, *Catal. Lett.*, 2009, **127,** 49-54.

14 T. Kolli, T. Kanerva, P. Lappalainen, M. Huuhtanen, M. Vippola, T. Kinnunen, K. Kallinen, T. Lepistö, J. Lahtinen, R. L. Keiski, *Top. Catal.*, 2009, **52,** 2025-2028.

15 S. Colussi, F. Arosio, T. Montanari, G. Busca, G. Groppi, A. Trovarelli, *Catal. Today*, 2010, **155,** 59-65.

16 M. Kärkkäinen, M. Honkanen, V. Viitanen, T. Kolli, A. Valtanen, M. Huuhtanen, K. Kallinen, M. Vippola, T. Lepistö, J. Lahtinen, R. L. Keiski, *Top. Catal.*, 2013, **56,** 672-678.

17 P. Tan, Z. Hu, D. Lou, *Fuel*, 2009, **88,** 1086-1091.

18 K. Zhang, J. Hu, S. Gao, Y. Liu, X. Huang, X. Bao, *Energy Policy*, 2010, **38,** 2934-2940.

19 M. Riad, S. Mikhai, *Catal. Sci. Technol.*, 2012, **2,** 1437-1466.

20 Y. Zheng, Y. Zheng, Y. Xiao, G. Cai, K. Wei, *Catal. Commun.*, 2012, **27,** 189-192.

21 H. Chang, J. Li, X. Chen, L. Ma, S. Yang, J.W. Schwank, J. Hao, *Catal. Commun.*, 2012, **27,** 54-57.

22 T. Paulson, B. Moss, B. Todd, C. Eckstein, B. Wise, D. Singleton, S. Zemskova, R. Silver, SAE paper 2008-01-2638, 2008.

23 F. Liu, H. He, C. Zhang, *Chem. Commun.*, 2008, 2043-2045.

24 J. Li, Y. Zhu, R. Ke, J. Hao, *Appl. Catal. B: Environ.*, 2008, **80,** 202-213.

25 J. A. Rodriguez, P. Liu, Y. Takahashi, F. Viñes, L. Feria, E. Florez, K. Nakamura, F. Illas, *Catal. Today*, 2011, **166,** 2-9.

26 C. Sun, J. Zhu, Y. Lv, L. Qi, B. Liu, F. Gao, K. Sun, L. Dong, Y. Chen, *Appl. Catal. B: Environ.*, 2011, **103,** 206-220.

27 X. Yao, Q. Yu, Z. Ji, Y. Lv, Y. Cao, C. Tang, F. Gao, L. Dong, Y. Chen, *Appl. Catal. B: Environ.*, 2013, **130-131,** 293-304.

28 Y. Kanno, T. Hihara, T. Watanabe, K. Katoh, M. Nagata, SAE paper 2004-01-1427, 2004.

29 G. Cavataio, H.W. Jen, J.W. Girard, D. Dobson, J.R. Warner, C.K. Lambert, SAE paper 2009-01-0627, 2009.

30 Z. Yang, Y. Chen, M. Zhao, J. Zhou, M. Gong, Y. Chen, *Chin. J. Catal.*, 2012, **33,** 819-826.

31 J. Andersson, M. Antonsson, L. Eurenius, E. Olsson, M. Skoglundh, *Appl. Catal. B: Environ.*, 2007, **72,** 71-81.

32 J. Aluha, G. Pattrick, E. Lingen, *Top. Catal.*, 2009, **52,** 1977-1982.

33 J. Kašpar, P. Fornasiero, N. Hickey, *Catal. Today*, 2003, **77,** 419-449.

34 K.M. Adams, J.V. Cavataio, R.H. Hammerle, *Appl. Catal. B: Environ.*, 1996, **10,** 157-181.

35 J. Kim, C. Kim, S. Choung, *Catal. Today*, 2012, **185,** 296-301.

36 A. Winkler, D. Ferri, M. Aguirre, *Appl. Catal. B: Environ.*, 2009, **93,** 177-184.

37 F.C. Galisteo, R. Mariscal, M.L. Granados, M.D.Z. Poves, J.L.G. Fierro, V. Kröger, R.L. Keiski, *Appl. Catal. B: Environ.*, 2007, **72,** 272-281.

38 C. Larese, M.L. Granados, F.C. Galisteo, R. Mariscal, J.L.G. Fierro, *Appl. Catal. B: Environ.*, 2006, **62,** 132-143.

39 J.M.A. Harmsen, J.H.B.J. Hoebink, J.C. Schouten, *Ind. Eng. Chem. Res.*, 2000, **39,** 599-609.

40 P. Bera, K.C. Patil, V. Jayaram, G.N. Subbanna, M.S. Hegde, *J. Catal.*, 2000, **196,** 293-301.

41 H. Oh, I. S. Pieta, J. Luo, W. S. Epling, *Top. Catal.*, 2013, **56,** 1916-1921.

42 K. Lee, E. Lee, C. Song, M. J. Janik, *J. Catal.*, 2014, **309,** 248-259.

43 S. Shwan, W. Partridge, J. S. Choi, L. Olsson, *Appl. Catal. B: Environ.*, 2014, **147,** 1028-1041.

44 S. Shwan, J. Jansson, J. Korsgren, L. Olsson, M. Skoglundh, *Catal. Today*, 2012, **197,** 24-37.

45 L. Olsson, M. Fredriksson, R. J. Blint, *Appl. Catal. B: Environ.*, 2010, **100,** 31-41.

46 D. Creaser, M. Nilsson, L. J. Pettersson, J. Dawody, *Ind. Eng. Chem. Res.*, 2010, **49,** 9712-9719.

47 A. Lindholm, N. W. Currier, J. Li, A. Yezerets, L. Olsson, *J. Catal.*, 2008, **258,** 273-288.

48 A. Lindholm, N. W. Currier, A. Yezerets, L. Olsson, *Top. Catal.*, 2007, **42-43,** 83-89.

49 J. Dawody, M. Skoglundh, L. Olsson, E. Fridell, *Appl. Catal. B: Environ.*, 2007, **70,** 179-188.

50 L. Olsson, H. Karlsson, *Catal. Today*, 2009, **147,** S290-S294.

51 X. P. Auvray, L. Olsson, *Ind. Eng. Chem. Res.*, 2013, **52,** 14556-14566.

52 X. P. Auvray, L. Olsson, *Catal. Lett.*, 2014, **144,** 22-31.

53 J. Dawody, I. Tonnies, E. Fridell, M. Skoglundh, *Top. Catal.*, 2007, **42-43,** 183-187.

54 S. Chansai, R. Burch, C. Hardacre, H. Oh, W. S. Epling, *Catal. Sci. Technol.*, 2013, **3,** 2349-2356.

55 M.E. Glávez, S. Ascaso, R. Moliner, M.J. Lázaro, *Chem. Eng. Sci.*, 2013, **87,** 75-90.

56 X. Guo, M. Meng, F. Dai, Q. Li, Z. Zhang, Z. Jiang, S. Zhang, Y. Huang, *Appl. Catal. B: Environ.*, 2013, **142-143,** 278-289.

57 L. Xie, F. Liu, K. Liu, X. Shi, H. He, *Catal. Sci. Technol.*, 2014, DOI: 10.1039/C3CY00924F.

58 F. Liu, W. Shan, Z. Lian, L. Xie, W. Yang, H. He, *Catal. Sci. Technol.*, 2013, **3,** 2699-2707.

59 X. Wang, A. Shi, Y. Duan, J. Wang, M. Shen, *Catal. Sci. Technol.*, 2012, **2,** 1386-1395.

60 M. Iwasaki, H. Shinjoh, *Appl. Catal. A: Gen.*, 2010, **390,** 71-77.

61 M. Schwidder, S. Heikens, A.D. Toni, S. Geisler, M. Berndt, A. Brückner, W. Grünert, *J. Catal.*, 2008, **259,** 96-103.

62 K. Rahkamaa-Tolonen, T. Maunula, M. Lomma, M. Huuhtanen, R.L. Keiski, *Catal. Today*, 2005, **100,** 217-222.

63 I.S. Pieta, M. García-Diéguez, M.A. Larrubia, L.J. Alemany, W.S. Epling, *Catal. Today*, 2013, **207,** 200-211.

64 W.S. Epling, L.E. Campbell, A. Yezerets, N.W. Currier, J.E. Parks II, *Catal. Rev.-Sci. Eng.*, 2004, **46,** 163-245.

65 H. Xu, Q. Zhang, C. Qiu, T. Lin, M. Gong, Y. Chen, *Chem. Eng. Sci.*, 2012, **76,** 120-128.

66 E. Litovsky, M. Shapiro, A. Shavit, *J. Am. Ceram. Soc.*, 1996, **79,**

1366-1376.

67 G. Ziegler, D.P.H. Hasselman, *J. Mater. Sci.*, 1981, **16,** 495-503.

68 Y. Wu, Q. Zhang, X. Yin, H. Cheng, *RSC Adv.*, 2013, **3,** 9670-9676.

69 A. Mattsson, C. Lejon, S. Bakardjieva, V. Štengl, L. Österlund, *J. Solid State Chem.*, 2013, **199,** 212-223.

70 Y. Wong, N. Wong, L. Shi, *J. Mater. Sci.*, 2003, **38,** 973-977.

71 L. Qi, C. Tang, L. Zhang, X. Yao, Y. Cao, L. Liu, F. Gao, L. Dong, Y. Chen, *Appl. Catal. B: Environ.*, 2012, **127,** 234-245.

72 L. Olsson, E. Fridell, *J. Catal.*, 2002, **210,** 340-353.

73 E.S. Putna, J.M. Vohs, R.J. Gorte, *Surf. Sci.*, 1997, **391,** L1178-1182.

74 J.Z. Shyu, K. Otto, *Appl. Surf. Sci.*, 1988, **32,** 246-252.

75 T. Huizinga, H.F.J. van't Blik, J.C. Vis, R. Prins, *Surf. Sci.*, 1983, **135,** 580-596.

76 A. D. Smeltz, W. N. Delgass, F. H. Ribeiro, *Langmuir*, 2010, **26,** 16578-16588.

77 E. Fridell, A. Amberntsson, L. Olsson, A. W. Grant, M. Skoglundh, *Top. Catal.*, 2004, **30,** 143-146.

78. J. J. Plata, A. M. Márquez, J. F. Sanz, R. S. Avellaneda, F. Romero-Sarria, M. I. Domínguez, M. A. Centeno, J. A. Odriozola, *Top. Catal.*, 2011, **54,** 219-228.

79. X.-Q. Gong, A. Selloni, O. Dulub, P. Jacobson, U. Diebold, *J. Am.*

Chem. Soc., 2007, **130,** 370-381.

80 C.D. Wagner, W.M. Riggs, J.F. Moulder, G.E. Muilenberg, Handbook of X-Ray Photoelectron Spectroscopy. Perkin-Elmer Corporation, Minnesota, 1979, pp. 98-99.

81 M.S. Kazi, M. Deeba, T. Neubauer, A.H. Punke, T.W. Mueller-Stach, G. Grubert, S.A. Roth, J.B. Hoke, S. Sung, Y. Li, X. Wei, C. Wan, US patent, 2010/0186375, 2010.

82 C.H. Kim, M. Schmid, S.J. Schmieg, J. Tan, W. Li, SAE paper 2011-01-1134, 2011.

83 A. Bentele, K. Wanninger, M. Gerd, M. Schneider, US patent, 2011/0311422, 2011.

Figure Captions

Fig. 1. The CO (a) and C_3H_6 (b) oxidation conversion over Pt/TiO_2, Pt/TiO_2-YO_x, Pt/TiO_2(A) and Pt/TiO_2-YO_x(A) catalysts.

Reaction conditions: C_3H_6: 330 ppm, CO: 1000 ppm, NO: 200 ppm, O_2: 10%, CO_2: 8%, vapor: 7%, SO_2: 50 ppm, N_2: balance, GHSV = 60,000 h^{-1}. All catalysts were pre-treated at 500 ^oC for 3h under the reaction atmosphere.

Fig.2. The CO (a) and C_3H_6 (b) oxidation conversion over Pt/TiO_2, Pt/TiO_2-YO_x, Pt/TiO_2(S) and Pt/TiO_2-YO_x(S) catalysts.

Reaction conditions: C_3H_6: 330 ppm, CO: 1000 ppm, NO: 200 ppm, O_2: 10%, CO_2: 8%, vapor: 7%, SO_2: 50 ppm, N_2: balance, GHSV = 60,000 h^{-1}. All catalysts were pre-treated at 500 ^oC for 3h under the reaction atmosphere.

Fig. 3. Arrhenius plots of the turnover frequecy (TOF) with respect to the total Pt amount on Pt/TiO_2, Pt/TiO_2-YO_x Pt/TiO_2(S) and Pt/TiO_2-YO_x(S) catalysts.

Reaction conditions: C_3H_6: 330 ppm, CO: 1000 ppm, NO: 200 ppm, O_2: 10%, CO_2: 8%, vapor: 7%, SO_2: 50 ppm, N_2: balance; flow rate: 2.5 L min^{-1}; GHSV = 60,000 h^{-1}.

Fig. 4. The conversion of NO to NO_2 over Pt/TiO_2 and Pt/TiO_2-YO_x catalysts.

Reaction conditions: C_3H_6: 330 ppm, CO: 1000 ppm, NO: 200 ppm, O_2: 10%, CO_2: 8%, vapor: 7%, SO_2: 50 ppm, N_2: balance, GHSV = 60,000 h^{-1}. All catalysts were pre-treated at 500 ^oC for 3h under the reaction atmosphere.

Fig. 5. The BJH pore size distribution curves of TiO_2, TiO_2-YO_x, TiO_2(A) and TiO_2-YO_x(A) supports.

Fig.6. SEM images of (a) Pt/TiO_2, (b) Pt/TiO_2-YO_x, (c) Pt/TiO_2(A) and (d) Pt/TiO_2-YO_x(A) catalysts.

Fig. 7. XRD patterns of TiO_2, TiO_2-YO_x, TiO_2(A) and TiO_2-YO_x(A) supports.

Fig. 8. (a) XPS (Pt 4f) spectra of Pt/TiO_2 and Pt/TiO_2-YO_x catalysts; (b) XPS (Pt 4f) spectra of Pt/TiO_2 and Pt/TiO_2-YO_x catalysts after three hours reaction; (c) XPS (Y 3d) spectra of Pt/TiO_2-YO_x catalyst.

Reaction conditions: C_3H_6: 330 ppm, CO: 1000 ppm, NO: 200 ppm, O_2: 10%, CO_2: 8%, vapor: 7%, SO_2: 50 ppm, N_2: balance, GHSV = 60,000 h^{-1}.

Fig. 9. HAADF-STEM images of (a) Pt/TiO_2, (b) Pt/TiO_2-YO_x catalysts; HR-TEM images of (c) Pt/TiO_2, (d) Pt/TiO_2-YO_x simples; (e) Pt particle size distributions of the both samples.

Table 1. Sulfur content deposited on Pt/TiO_2, Pt/TiO_2-YO_x and commercial DOC catalysts.

Samples	Sulfur content (wt.%)
Pt/TiO_2(A)	1.3
Pt/TiO_2(S)	1.7
Pt/TiO_2-YO_x(A)	1.8
Pt/TiO_2-YO_x(S)	2.3
Pt/Al_2O_3(A) [a]	5.8
Pt/Al_2O_3(S) [a]	5.8
Pt-Pd/CeO_2-ZrO_2-Al_2O_3(A) [a]	4.4
Pt-Pd/CeO_2-ZrO_2-Al_2O_3(S) [a]	4.8

[a] Commercial DOC was supplied by Sichuan Zhongzi Exhaust Purge Co. Ltd.

Table 2. CO and C_3H_6 reaction rates and apparent activation energies over Pt/TiO_2, Pt/TiO_2-YO_x, Pt/TiO_2(S) and Pt/TiO_2-YO_x(S) catalysts.

Catalysts	Reactant	Reaction rate (mol g^{-1} s^{-1})		TOF (s^{-1})		Ea (kJ mol^{-1})	
Pt/TiO_2	CO	[a] 1.40×10^{-6}	[b] 1.94×10^{-6}	0.0272 [a]	0.0377 [b]	180.8 [a]	183.5 [b]
Pt/TiO_2(S)		[a] 1.31×10^{-6}	[b] 1.94×10^{-6}	0.0256 [a]	0.0377 [b]	181.5 [a]	183.9 [b]
Pt/TiO_2-YO_x		[a] 1.97×10^{-6}	[b] 3.29×10^{-6}	0.0383 [a]	0.0641 [b]	78.7 [a]	78.4 [b]
Pt/TiO_2-YO_x(S)		[a] 1.80×10^{-6}	[b] 3.21×10^{-6}	0.0350 [a]	0.0626 [b]	95.7 [a]	95.5 [b]
Pt/TiO_2	C_3H_6	[c] 1.51×10^{-7}	[d] 4.46×10^{-7}	0.0029 [c]	0.0087 [d]	197.1 [c]	196.8 [d]
Pt/TiO_2(S)		[c] 1.43×10^{-7}	[d] 4.01×10^{-7}	0.0028 [c]	0.0078 [d]	198.1 [c]	198.1 [d]
Pt/TiO_2-YO_x		[c] 5.73×10^{-7}	[d] 15.5×10^{-7}	0.0112 [c]	0.0302 [d]	155.6 [c]	154.9 [d]
Pt/TiO_2-YO_x(S)		[c] 5.28×10^{-7}	[d] 12.9×10^{-7}	0.0103 [c]	0.0251 [d]	165.6 [c]	165.4 [d]

The Pt content on each catalyst is 5.13×10^{-5} mol g^{-1}.

[a] Catalyst bed temperature = 190 °C.

[b] Catalyst bed temperature = 200 °C.

[c] Catalyst bed temperature = 205 °C.

[d] Catalyst bed temperature = 215 °C.

Table 3. Texture properties of TiO_2 and TiO_2-YO_x surports.

Samples	Surface Area (m^2/g)	Pore Volume (cm^3/g)	Average Pore Diameter (nm)
TiO_2	98	0.22	8.6
TiO_2-YO_x	155	0.28	7.2
TiO_2(A)	32	0.13	16.8
TiO_2-YO_x(A)	66	0.26	15.4

[a] TiO_2 and TiO_2-YO_x samples were calcined 3h at 500 ^oC.

[b] TiO_2(A) and TiO_2-YO_x(A) samples were calcined 3h at 700 ^oC.

Table 4. Experimentally obtained XPS peak positions of Y (eV)

Samples	Preparation method	Y $3d_{5/2}$	Y $3d_{3/2}$
TiO_2-YO_x	co-precipitaion	157.5	159.4
Y_2O_3	co-precipitaion	156.8	158.7
Y_2O_3	Reference [80]	156.4	158.2

Fig.1(a) and 1(b)

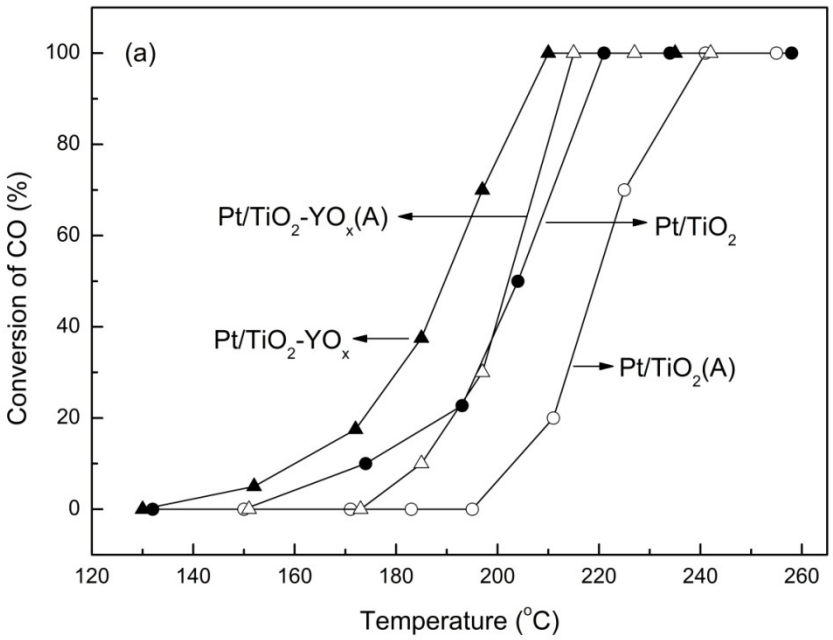

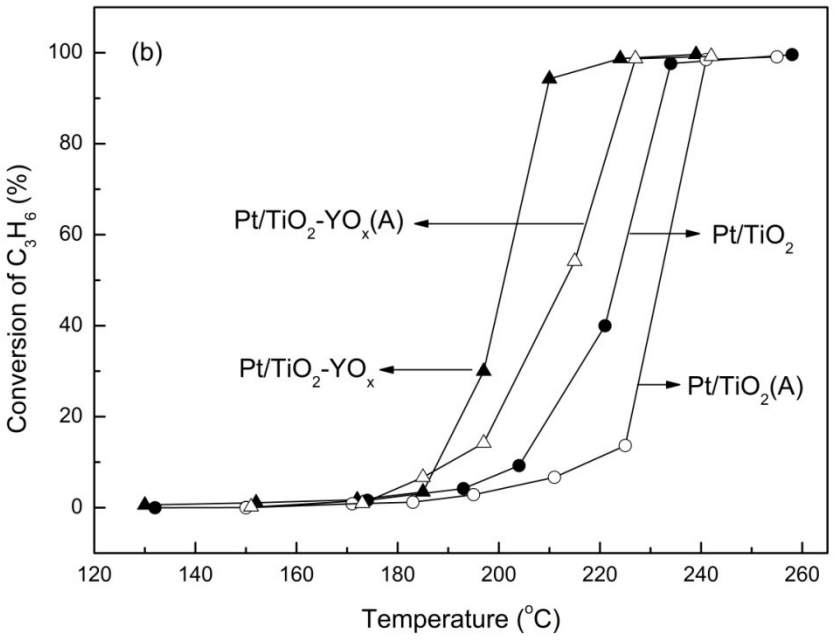

Fig. 2(a) and 2(b)

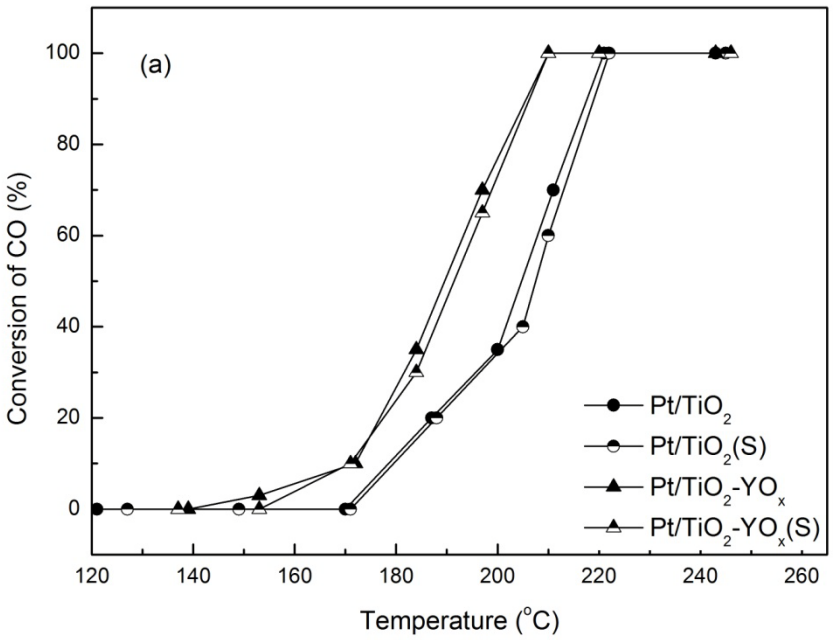

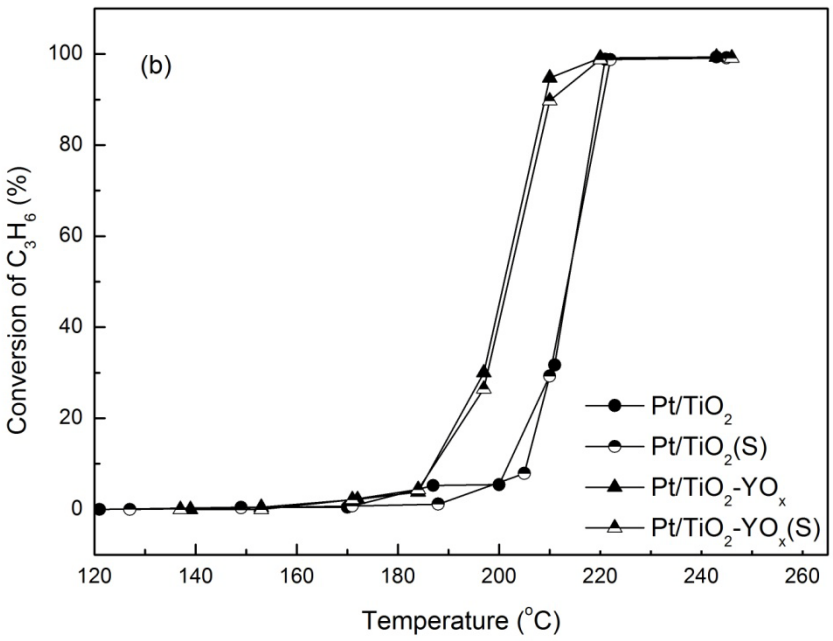

Fig. 3(a) and 3(b)

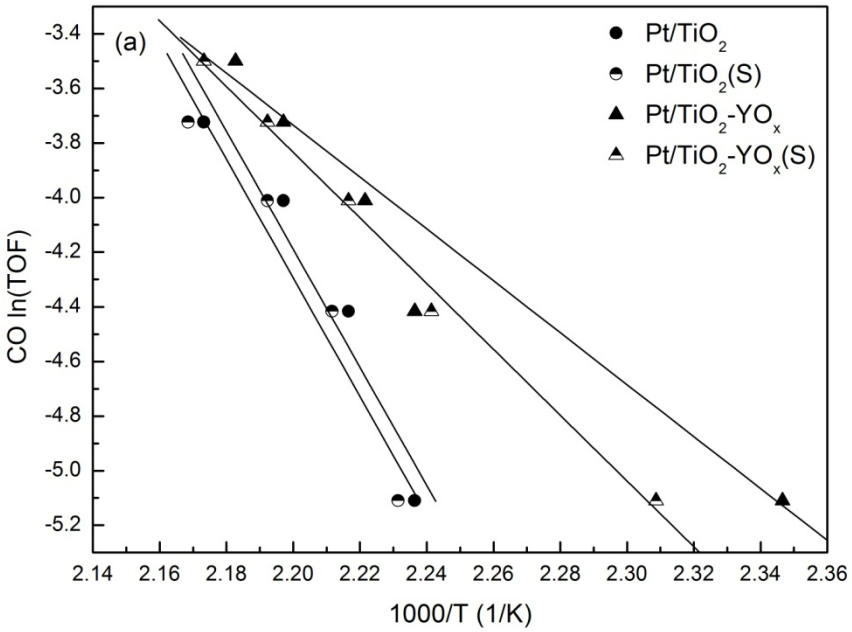

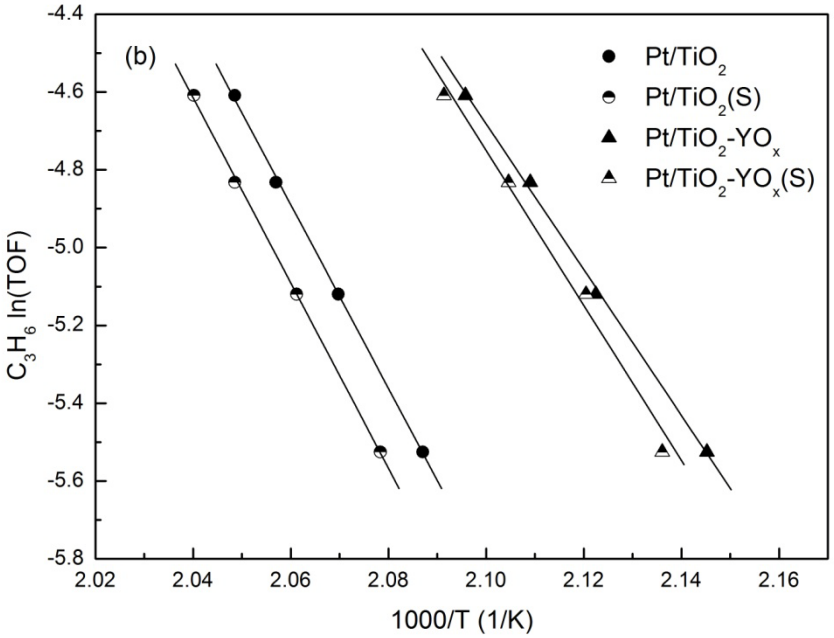

Fig. 4.

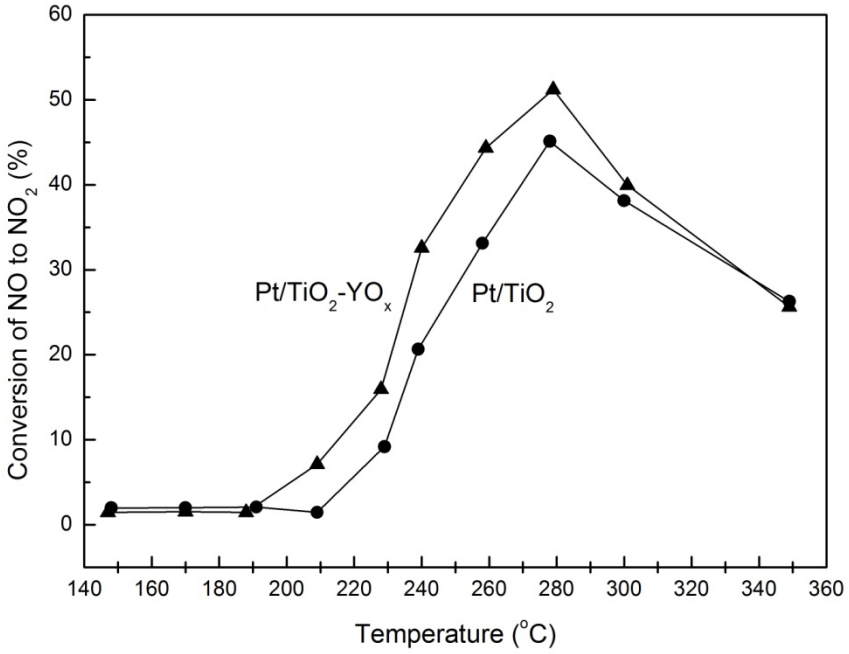

Fig. 5

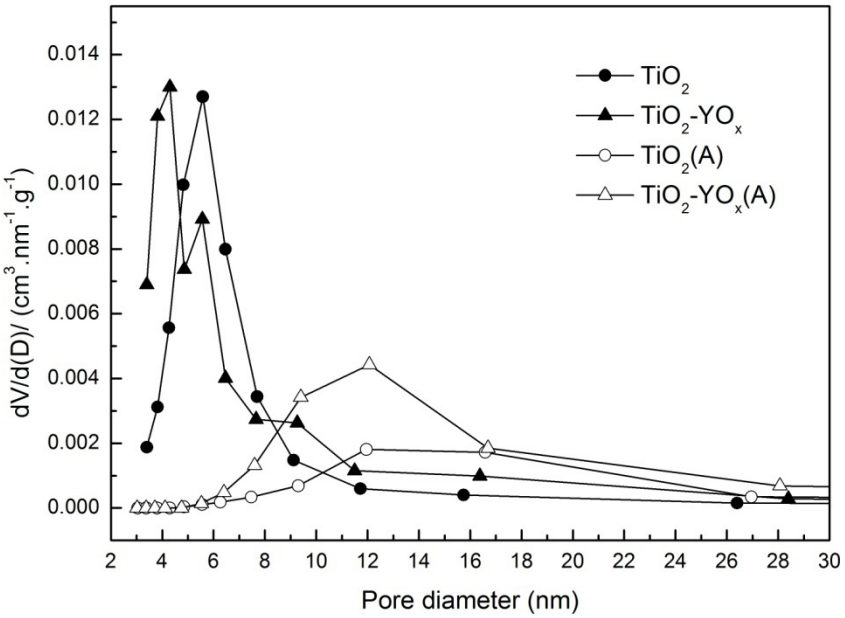

Fig.6(a)-6(d)

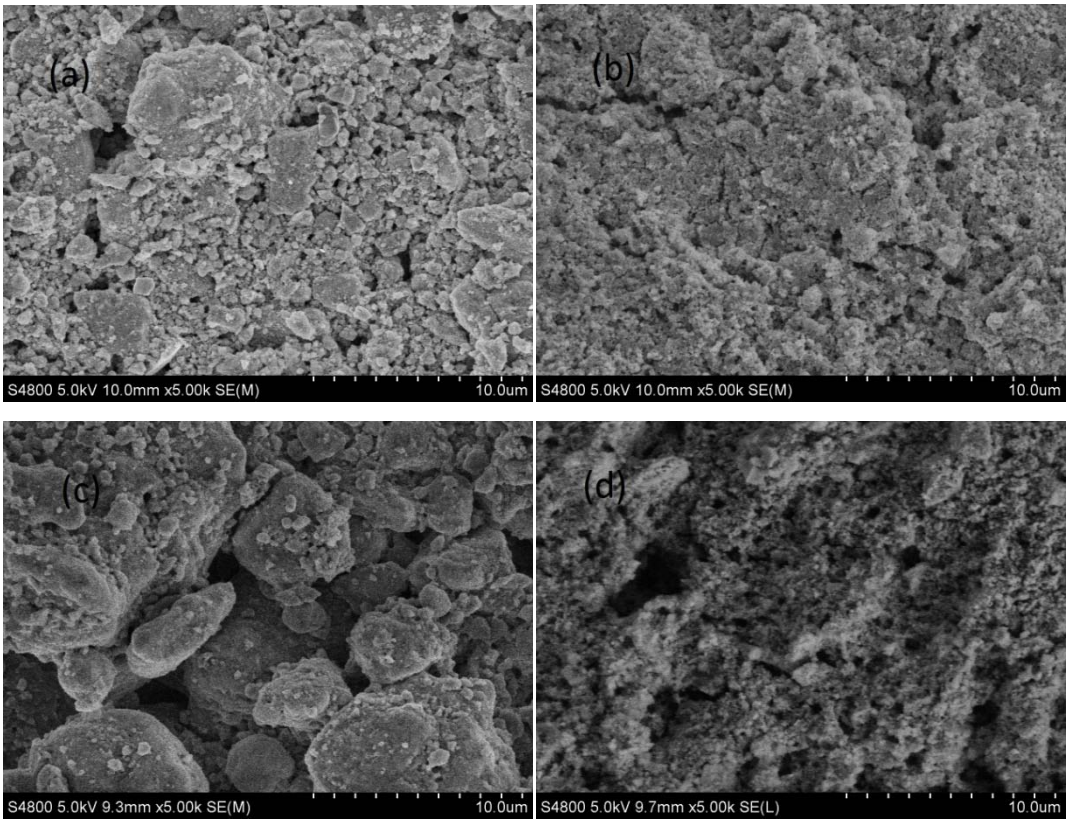

Fig.7

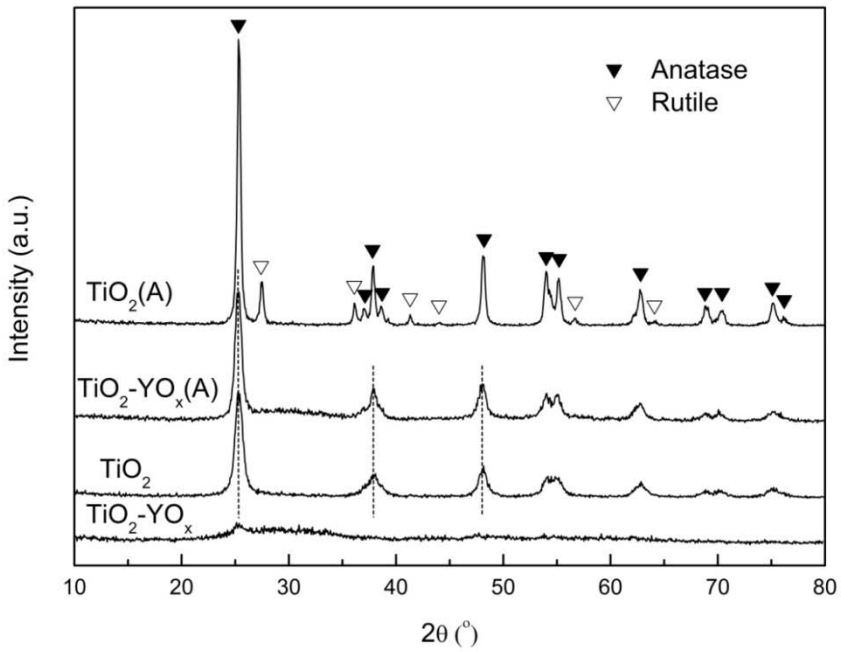

Fig.8(a), 8(b) and 8(c)

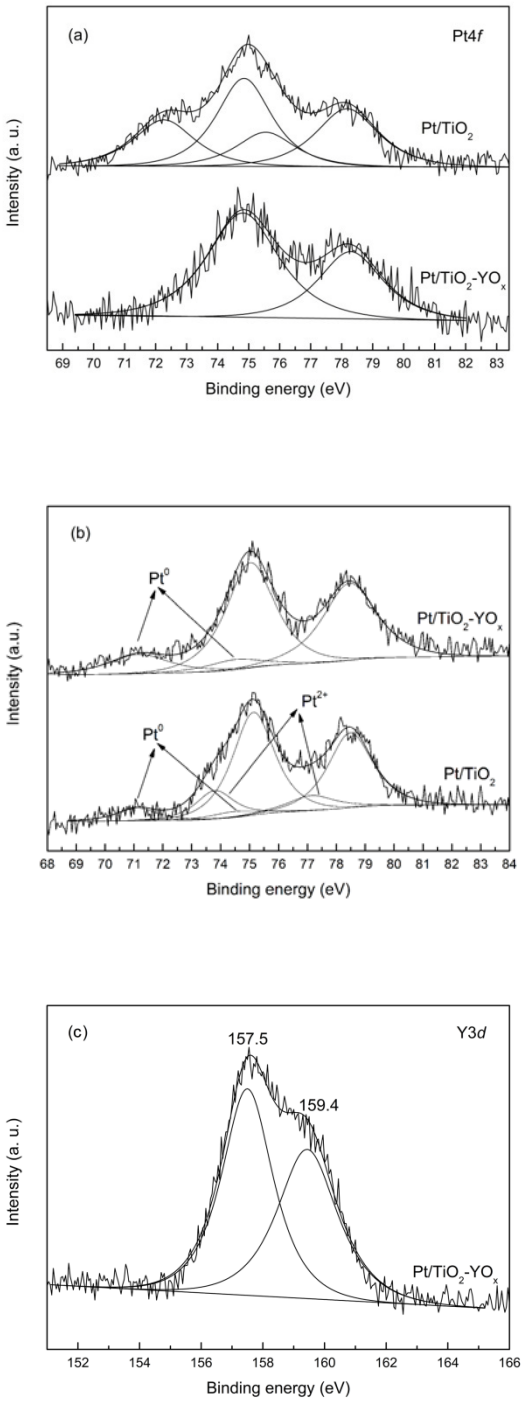

Fig.9(a)-9(e)